Optical reflectance study of the electronic structure of acceptor-type graphite intercalation compounds

D. M. Hoffman, R. E. Heinz,* G. L. Doll, and P. C. Eklund
Department of Physics and Astronomy, University of Kentucky, Lexington, Kentucky 40506
(Received 26 December 1984)

We have measured the absolute reflectance at near-normal incidence of stage-1—4 graphite-$SbCl_5$ intercalation compounds in the photon-energy range 0.08—10 eV and have subsequently performed a Kramers-Kronig phase-shift analysis of the data. A separation of free- and bound-charge contributions to the optical dielectric function $\epsilon(0,\omega)$ is carried out to extract values for the free-carrier (Drude) parameters, charge transfer between intercalate and carbon layers, Fermi-level positions, and important interband transition energies associated with both valence-band—to—valence-band and valence-band—to—conduction-band absorption in the perturbed carbon π bands. The optical results are compared to previously published two-dimensional energy-band calculations.

I. INTRODUCTION

We report the results of optical studies on graphite intercalation compounds (GIC's) (Refs. 1 and 2) formed by the reaction of the Lewis acid $SbCl_5$ with graphite. These compounds form unusually stable examples of acceptor-type GIC's which can, for most experimental studies, be handled in laboratory air.[3] Stage-1—6 compounds can be prepared, where the stage index refers to the number of carbon layers which separate the periodically inserted molecular layers. As a consequence of this air stability, this GIC system is now one of the most heavily studied.[1,2,4] The intercalation chemistry of graphite-$SbCl_5$ and the related GIC systems formed by reaction with SbF_5 and AsF_5 have been described in terms of the disproportionation of MX_5 into MX_3 and MX_6^-, where $M=$Sb,As and $X=$Cl,F.[5] This reaction need not go to completion and therefore concentrations of the various products or adducts (e.g., $SbCl_5$, $SbCl_6^-$, $SbCl_3$, $SbCl_4^-$, and $SbCl_5\cdot SbCl_6^-$) (Refs. 6—9) may be found in the intercalate layers depending on the sample preparation. Recent high-resolution scanning transmission electron microscope (STEM) studies of stage-4 graphite-$SbCl_5$ by Huang, Qian, and Solin[10] report clear evidence for segregated phases of differing [Sb]/[Cl] ratio. Islands of diameters 500—1000 Å were observed (stoichiometry $SbCl_{3.2}$) amidst a sea of reported stoichiometry $SbCl_{7\pm2}$.[10] The islands, which were found to account for $\sim 11\%$ of the sample area, are reported to be disordered, yielding diffuse rings in microdiffraction studies, whereas the sea or background exhibits a pattern which is identified with $(\sqrt{7}\times\sqrt{7})R\,19.1°$ structure. Of particular significance to our spectroscopic studies, which cannot resolve spatially this microstructure, is the STEM observation[10] of the spatial invariance of the carbon $1s$ core excitation. This invariance suggests equal carbon π-band contributions to the dielectric function from the island and background regions. Further STEM studies are needed to determine if these islands occur in samples prepared under different (e.g., higher temperature) conditions.

To study quantitatively the electronic properties of the graphite-$SbCl_5$ compounds we have collected absolute reflectance data on the stage-1—4 compounds over the energy range 0.08—10 eV. This energy range is sufficient to determine the optical dielectric function $\epsilon(0,\omega)$ by Kramers-Kronig techniques. A successful separation of free-carrier and bound-charge contributions to $\epsilon(0,\omega)$ yields a considerable amount of information regarding charge transfer and band structure of the stage-1—4 compounds (e.g., plasma frequency, carrier lifetime, Fermi level, and valence-band energy differences). We interpret the separate contributions to the dielectric function in terms of two-dimensional (2D) energy-band model calculations by Blinowski and co-workers[11,12] and Ohno, Shima, and Kamimura.[31]

II. EXPERIMENTAL DETAILS

Stage-1—4 graphite-$SbCl_5$ samples were prepared using highly oriented pyrolytic graphite (HOPG) supplied by Union Carbide and $SbCl_5$ (Alpha Products, Inc.). The $SbCl_5$ was distilled into Pyrex reaction ampoules containing HOPG and sealed off. Stages 2—4 were grown in the vapors of $SbCl_5$ by the two-temperature technique as described previously;[3] the stage-1 compound, which is much more difficult to prepare successfully, was grown by submersion in liquid $SbCl_5$ at 90 °C for 3 d. It appears that stage-1 graphite-$SbCl_5$ compounds form more readily when thin ($\sim 200\,\mu$m) slabs of graphite (HOPG) are used.[14]

The stage index of each sample was characterized using both $(00l)$ x-rays (bulk) and Raman spectroscopy (~ 1000—Å probe depth). The c-face probe depth in the Raman experiments is comparable to the probe depth in the middle-ir—vacuum-uv region covered in the present spectroscopic study. The $(00l)$ scans of the stage-1—4 samples are shown in Fig. 1. Raman spectra in the 1600-cm^{-1} region (insets to Fig. 1) contain the intercalation-perturbed, high-frequency intralayer graphitic modes.[1,2,15] The x-ray data were taken with a General Electric XRD-6 diffractometer equipped with a Si:Li detector and Mo $K\alpha$

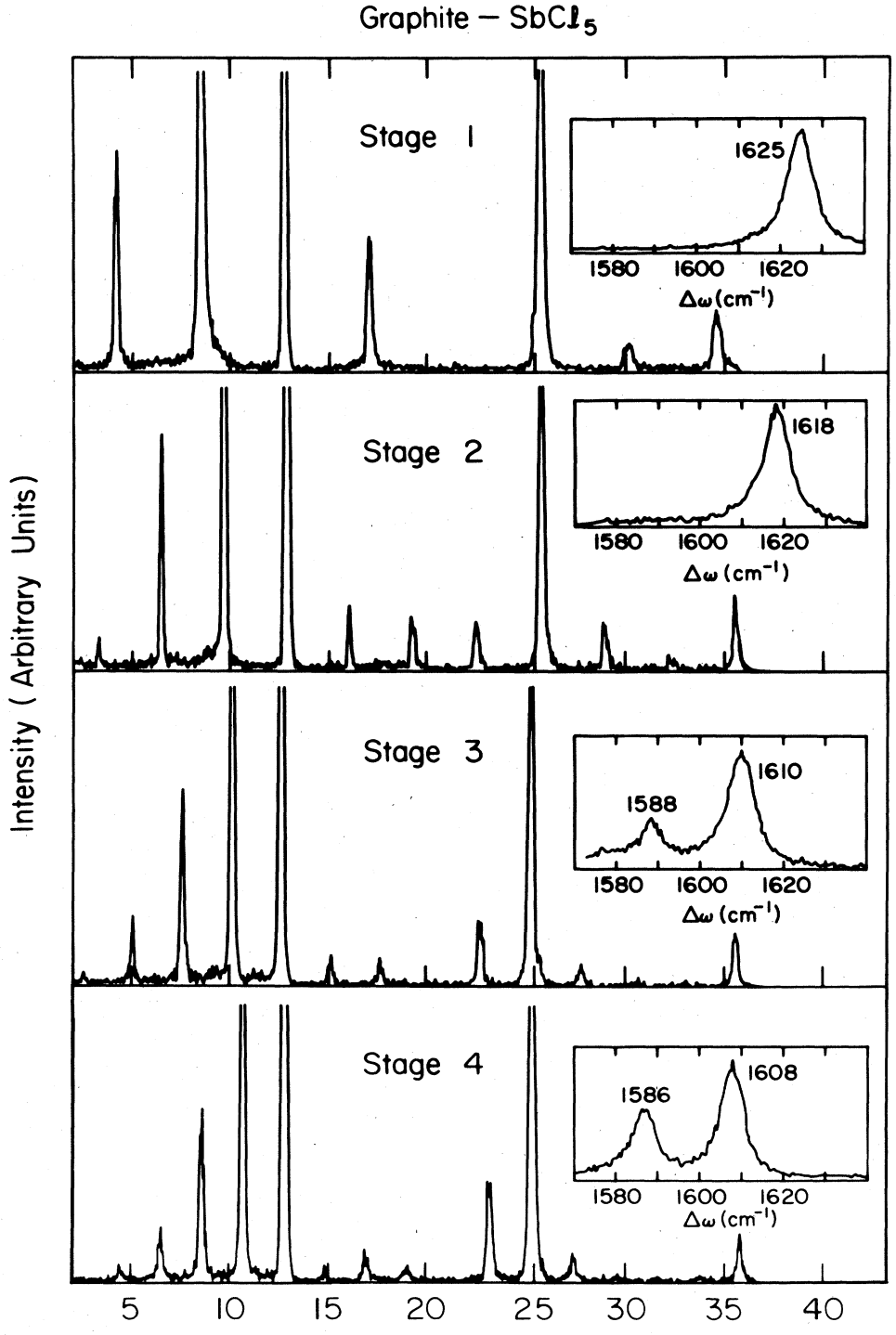

FIG. 1. X-ray (00l) scans and Raman spectra (insets) of the high-frequency intralayer phonons of stage-1—4 graphite-$SbCl_5$. Both experiments are stage specific but probe different depths: Mo $K\alpha$ x rays ~ 50 μm, argon laser ~ 1000 Å. The optical reflectivity experiments also probe depths of ~ 1000 Å.

source. Narrow (00l) peaks with no discernible shoulders indicate that the bulk of the sample is substantially single-stage material. The c-axis repeat distances observed were in good agreement with the literature.[16,17]

The Raman spectra of the E_{2g} Γ-point graphitic phonons in the ~ 1600-cm^{-1} region have been shown to be stage specific, exhibiting peaks identified with carbon intralayer modes in bounding and interior carbon layers. Thus for stages $n > 2$ a doublet is observed with the low- and high-frequency components identified with the interi-

or and bounding layers, respectively.[1,2,15] Although it is difficult to rule out ~10% admixture of a second phase (stage) on the basis of a Raman spectrum, the probe is nevertheless of considerable significance to optical reflectance studies since even the majority stage index in the first 1000 Å below the sample c face need not match the stage index in the bulk.[18] The Raman spectra were collected in the Brewster-angle backscattering geometry using Ar-ion laser radiation at low power (50—100 mW). Details of the Raman equipment are given elsewhere.[19] Raman spectra were collected on the samples before and after the reflectance spectra were taken to monitor any changes in the samples. Only the stage-1 samples were observed to undergo a change, exhibiting an asymmetric broadening of the initial Lorentzian line shape. This broadening is interpreted as a partial deintercalation near the c face to form small admixtures of stage-2 material. This interpretation is borne out by the reflectance studies which reveal a stage-2 feature at 0.375 eV in the otherwise flat region of the stage-1 spectrum. That stage 1 is not completely stable near the surface under the described experimental conditions is not too surprising in view of the difficulty in preparing the compound.

Spectra were collected over the photon energy range 0.08—6 eV with the samples bathed in a flow of dry N_2. A $\frac{1}{4}$-m grating monochromator (SPEX No. 1670) with glowbar and W-filament sources, three gratings, order-sorting filters, and a pyroelectric detector were used in the infrared region from 0.08 to 0.65 eV. A prism monochromator (Perkin Elmer No. 83) with calcium fluoride and quartz prisms, W-filament and deuterium sources, and pyroelectric and silicon photodiode detectors was used to cover the region 0.5—6.0 eV. In each of these two spectrometers the reflectance was determined using single-beam optics by substituting a standard reflector (e.g., Au, Ag, or MgF_2-coated Al mirrors) at each wavelength. The absolute reflectance scale was checked at 1.96 eV using a He-Ne laser. Reflectance spectra above 5 eV were taken using a vacuum-ultraviolet monochromator (McPherson No. 225) equipped with a hydrogen capillary discharge source and a diffusion-pumped sample chamber containing a computer-controlled light-pipe detector. Standard reflectors were therefore not needed in the (5—10)-eV range.

III. RESULTS AND DISCUSSION

A. Kramers-Kronig analysis

The optical reflectance spectra of stage-1—4 graphite-$SbCl_5$ and HOPG in the energy range 0.08—10 eV are shown in Fig. 2. The dashed lines in the spectra represent the calculated reflectance from the free-carrier and low-energy interband contributions to the dielectric function. The details of this calculation are discussed in Sec. III B. The GIC spectra in the figure compare favorably with those reported previously in the energy range 0.2—2.5 eV by Eklund, Smith, and Murthy.[20] The inset to each spectrum shows the low-energy region on an expanded scale where structure associated with valence-band—to—valence-band ($V \rightarrow V$) transitions is anticipated for stage $n > 1$.

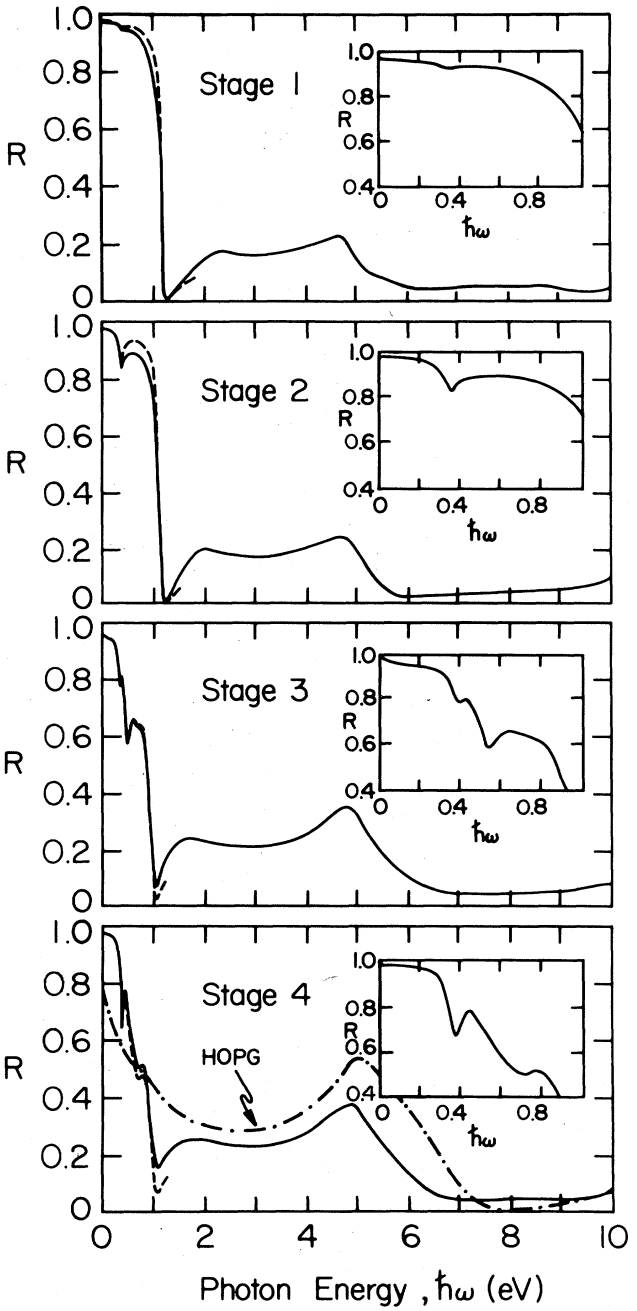

FIG. 2. Reflectance data measured at near-normal incidence to the c face of stage-1—4 graphite-$SbCl_5$ and HOPG. The dashed lines represent the reflectance calculated from the free-carrier [Drude, Eq. (3)] and low-energy interband transition [$V \rightarrow V$, Eq. (5)] contributions. All parameters are given in Table I. The reflectance of HOPG is shown as the dashed-dotted line in the bottom panel. The insets show the low-photon-energy region where the structure is due to valence-to-valence interband transitions.

The weak feature in the inset to the stage-1 spectrum is due to a small inclusion of stage-2 material in the skin

depth. Freshly cleaved stage-1 samples show no evidence of this feature. The prominent feature in each GIC spectrum is the sharp "Drude" edge located near ~ 1 eV which is characteristic of metallic conduction. The Drude edges are "pinned" near ~ 1 eV by strong interband absorption at slightly higher energies which is associated with valence-band—to—conduction-band ($V \rightarrow C$) transitions. The intraband and interband contributions to the spectra are best discussed in terms of the dielectric function $\epsilon(\omega)=\epsilon_1(\omega)+i\epsilon_2(\omega)$, which can be obtained from the data by a Kramers-Kronig phase-shift analysis. Following standard procedures the experimental data were first extended to lower and higher photon energies in order to calculate the phase-shift integral given by[21]

$$\theta(\omega)=\frac{\omega}{\pi}\int_0^\infty \frac{\ln[R(\omega')/R(\omega)]}{\omega^2-\omega'^2}d\omega' . \quad (1)$$

Consistent with the conductive nature of the GIC's and HOPG, the data were extended to lower energies in terms of a Drude model for intraband absorption.[22] Above ~ 10 eV the energy-band structure of pristine graphite is determined primarily by intralayer interactions;[23] the GIC spectra were therefore extended in the (10—25)-eV region as a scaled spectrum of pristine graphite. The stage-dependent scale factors were chosen to reflect the intercalation-induced change in the c-axis density of the carbon layers. Above 25 eV the spectra were continued as ω^{-4}, characteristic of free electrons.[24]

The dielectric function $\epsilon(\omega)$ and related functions are then calculated directly from the phase-shift integral [Eq. (1)] without further approximation. The results for the real and imaginary part of the dielectric function [$\epsilon_1(\omega)$, $\epsilon_2(\omega)$], the electron-energy-loss function (Im$[-1/\epsilon(\omega)]$), and the real part of the bound-charge contribution to the optical conductivity σ_1 ($\sigma_1=\omega\epsilon_2/4\pi$) for stage-1—4 graphite-$SbCl_5$ and HOPG are shown in Figs. 3(a)—3(e). In the next section we discuss the method of separation of the bound- and free-charge contributions to the dielectric function. The results for HOPG shown in Fig. 3(e) are in good agreement with those previously published for single-crystal graphite by Taft and Phillip.[25]

B. Separation of intraband and interband contributions

Both the semimetallic HOPG and the metallic GIC's will have both free-carrier and bound-charge contributions to the dielectric function $\epsilon(0,\omega)$,

$$\epsilon(0,\omega)=\epsilon^{\text{free}}(\omega)+\epsilon^{\text{bound}}(\omega) . \quad (2)$$

The free-carrier or intraband contribution is described in the Drude approximation as

$$\epsilon^{\text{free}}(\omega)=\epsilon_\infty-\frac{\omega_p^2}{\omega(\omega+i/\tau)} , \quad (3)$$

where ω_p, τ, and ϵ_∞ are the plasma frequency, carrier lifetime, and core dielectric constant, respectively.

Several model band-structure calculations applicable to the graphite-$SbCl_5$ compounds have been published.[11—13,26—28] We shall examine our data in light of the calculations of Blinowski and co-workers[11,12] and Ohno *et al.*[13] These authors consider the GIC as a two-dimensional carbon layer sandwich bounded by intercalate layers, which eliminates all c-axis dispersion in the electronic energy bands. Weak c-axis dispersion occurs if a small interaction between intercalate and bounding carbon layers is considered, and this interaction has been shown to broaden and shift slightly the low-energy interband features in ϵ_2.[29] c-axis interaction between carbon layers bounded between successive intercalate layers is considered in the 2D sandwich models, however, and for a stage-n compound these interactions lead to a set of n conduction and n valence bands located near each corner of the hexagonal Brillouin zone.[11,12,13,27]

For the purpose of understanding the origin of the various intraband and interband contributions to the dielectric function of the stage-1—4 GIC's, we schematically represent in Fig. 4 the 2D model results for a stage-n compound. Plotted in the figure is the electronic energy versus in-plane wave vector measured relative to the corner of the hexagonal Brillouin zone. No attempt is made in the figure to display the correct shapes of the bands near their maxima or minima. The exact mirror symmetry of the conduction and valence bands implied by the figure is only obtained for the stage-1 and -2 compounds, or in the stage-3 and -4 compounds under the assumption that all holes created in the carbon π bands reside only in the bounding carbon layers.[12,13,27,28] If the holes reside mainly in the bounding layers with some fraction (~ 0.1) residing in the interior layers, the exact mirror symmetry between conduction and valence bands is lost.[12,13,28] The Fermi level is shown in the figure below the highest valence-band maxima consistent with the production of holes by charge transfer of electrons to lower-lying acceptor states identified with the intercalate layers. Metallic conduction is supported by the partially occupied bands in the figure and the resulting hole plasma gives rise to intraband absorption which dominates the dielectric function at the lowest energies. Interband absorption between π bands in the p-type acceptor GIC's is identified[11,12] with low-energy transitions ($V \rightarrow V$) between approximately parallel valence bands and higher-energy transitions ($V \rightarrow C$) between valence and conduction bands as indicated in the figure. Consistent with the mirror symmetry or near mirror symmetry in the band structure, there is a threshold for $V \rightarrow C$ absorption at $\sim 2E_F$, where the Fermi energy E_F is measured from the midpoint between the conduction- and valence-band manifolds. Furthermore, since nearly parallel valence and parallel conduction bands are obtained,[11—13,27,28] sharp $V \rightarrow V$ structure is anticipated at energies identifiable with valence-band energy differences. We therefore write the bound-charge contribution as[20]

$$\epsilon^{\text{bound}}(\omega)=\epsilon^{V\rightarrow V}(\omega)+\epsilon^{V\rightarrow C}(\omega) , \quad (4)$$

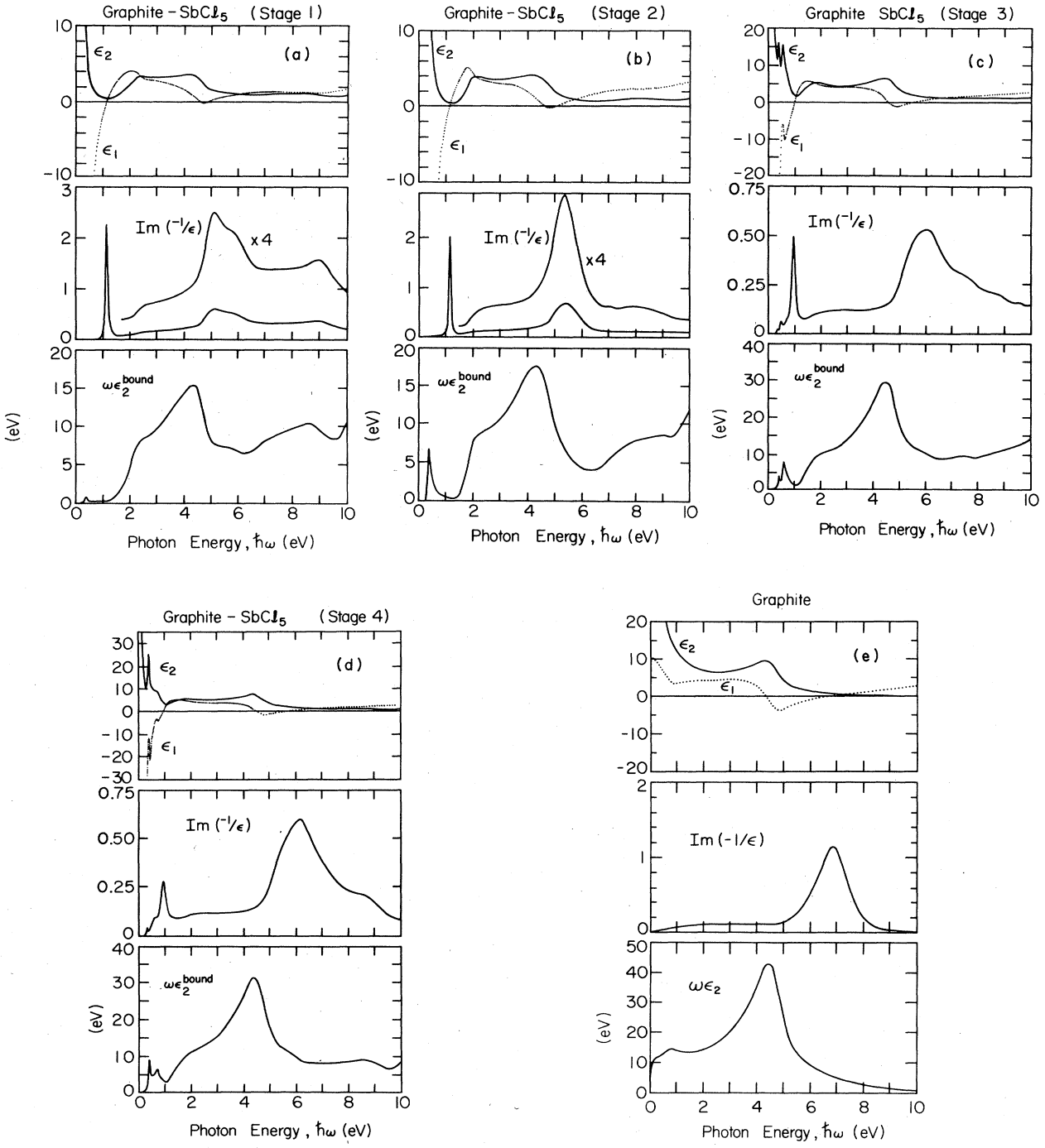

FIG. 3. (a)—(e) real (ϵ_1) and imaginary (ϵ_2) dielectric functions, electron-energy-loss function [Im$(-1/\epsilon)$], and the real part of the conductivity σ_1 due to bound charges only ($4\pi\sigma_1=\omega\epsilon_2$) based on the Kramers-Kronig analysis of the reflectance data shown in Fig. 2.

where $\epsilon^{V\to V}$ and $\epsilon^{V\to C}$ are the terms describing absorption due to vertical transitions between the respective bands. The free-carrier and bound-charge contributions are readily separated at energies $\hbar\omega < 2E_F$ below the threshold for $V\to C$ absorption because the low-energy $V\to V$ structure is sharp. We write the $V\to V$ term as a sum of Lorentzians,[20]

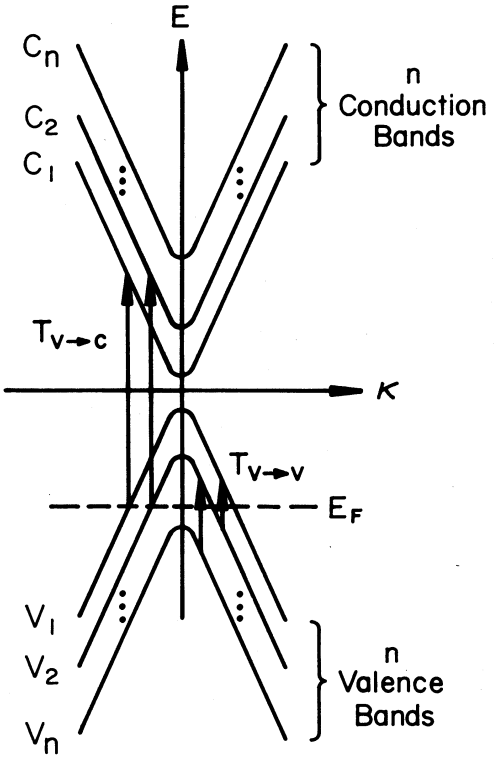

FIG. 4. Schematic representation of the two-dimensional energy-band structure for a stage-n compound near the zone corner of the hexagonal Brillouin zone. The dashed line indicates the position of the Fermi level, which has been lowered relative to the point of mirror symmetry due to charge transfer from the graphite to lower-lying intercalant-derived states. Interband transitions between valence bands ($V\to V$) and valence to conduction bands ($V\to C$) are indicated by arrows.

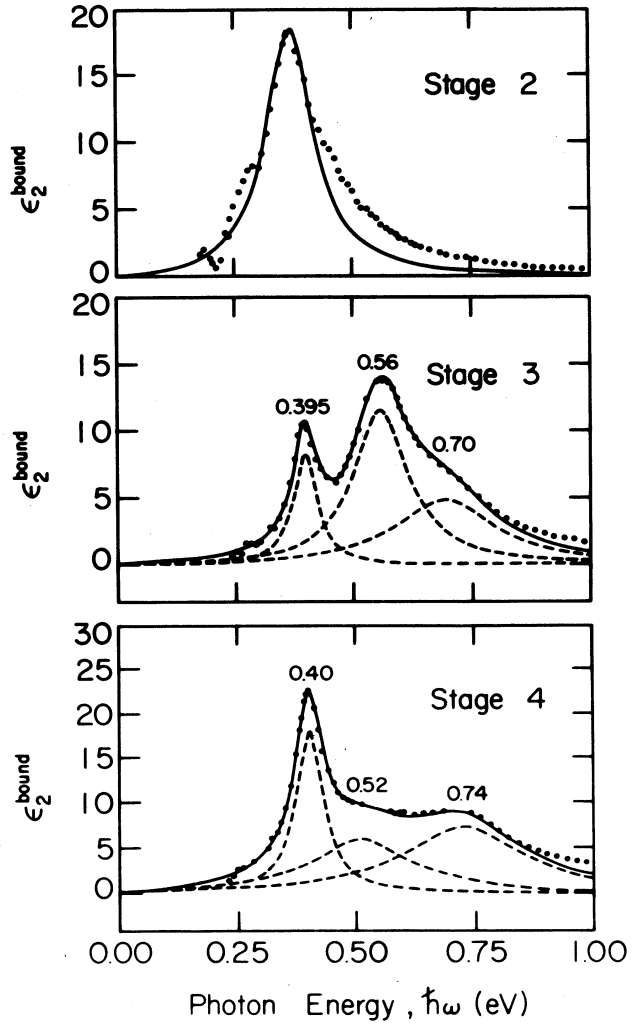

FIG. 5. ϵ_2 due to valence-to-valence interband transitions determined from the separation of free- and bound-charge contributions for stag-2—4 graphite-$SbCl_5$. The dashed lines indicate the individual Lorentzians calculated using Eq. (5). The Lorentzian parameters are given in Table I. The solid line indicates the resulting fit to the data shown as dots.

$$\epsilon^{V\to V}(\omega)=\sum_{i,j}{}' \frac{f_{ij}}{(\omega_{ij}^2-\omega^2)+i\Gamma_{ij}\omega} , \tag{5}$$

where f_{ij} is the oscillator strength, $\hbar\omega_{ij}$ is the energy difference, and Γ_{ij} is the effective width of the absorption band resulting from transitions between valence bands V_i and V_j. Lorentzian functions are well known to satisfy the Kramers-Kronig relations linking ϵ_1 and ϵ_2. For energies $\hbar\omega < 2E_F$, we fit the function $\epsilon^{free}+\epsilon^{V\to V}$ to the data ϵ_2 obtained from the phase-shift analysis. The results of this analysis are shown in Figs. 5 and 6. In Fig. 5 we plot (dots) $\epsilon_2^{bound}=\epsilon_2-\epsilon_2^{free}$. The calculated $V\to V$ term representing the low-energy contribution to ϵ_2^{bound} is indicated by the solid line; the dashed lines represent the individual Lorentzian functions. As can be seen in the figure, the $V\to V$ structure is sharp and reasonably well described by Lorentzian(s).

When plotted as $(\omega\epsilon_2)^{-1}$ versus $(\hbar\omega)^2$, the Drude model for free carriers results in a straight line. In Fig. 6 we plot $\epsilon_2(\omega)$ in the low-energy ($\hbar\omega \leq 0.5$ eV) region in this way. The data are represented by dots, the calculated free-carrier contribution [Eq. (3)] is indicated by the solid line, and the dashed line corresponds to the calculated sum [Eqs. (3) and (5)] of the free-carrier and low-energy interband terms. As can be seen in the figure, the data asymptotically approach at low energy the straight line representing the calculated free-carrier term. At higher energies the departure from this linear behavior is caused by the $V\to V$ interband contribution. Over the entire energy range of Fig. 6 the $\epsilon_2(\omega)$ data are, however, well described by the calculated sum of the free-carrier and $V\to V$ contributions. The parameters used to describe these contributions appear in Table I, and are also used to calculate the low-energy reflectance (dashed lines) of the stage-1—4 compounds appearing in Fig. 2.

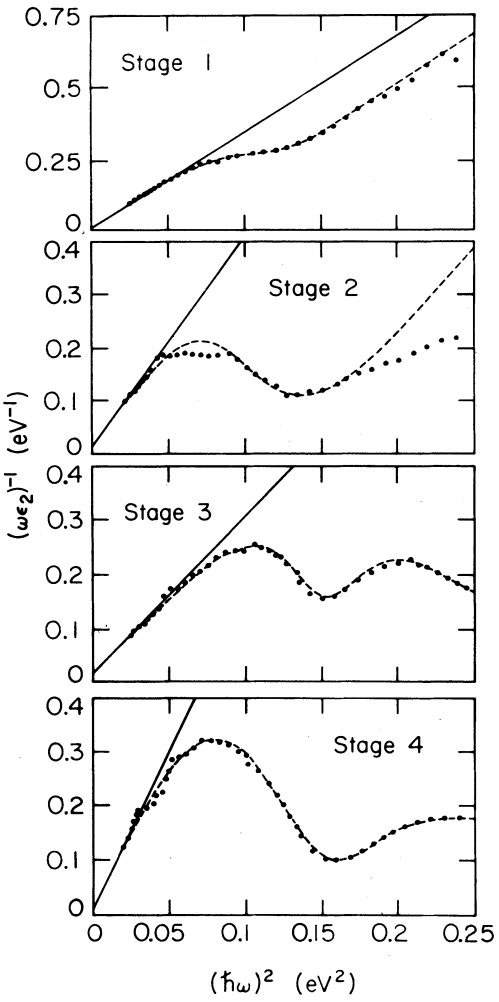

FIG. 6. Plot of $(\omega\epsilon_2)^{-1}$ vs $(\hbar\omega)^2$ for $\hbar\omega \leq 0.5$ eV. Free-carrier absorption well described by the Drude model appears as a straight line in this type of plot. Deviations from linear behavior are due to valence-to-valence interband transitions. The dots are the data, the solid line is the Drude term only [Eq. (3)], and the dashed line are the calculated Drude plus valence-to-valence interband transition contribution [Eq. (5)]. All parameters are given in Table I.

C. Intraband absorption

In Fig. 7 we plot the square of the plasma frequency (ω_p^2) versus inverse stage index $(1/n)$ for stage-1–4 graphite-$SbCl_5$ and stage-1–6 graphite-$FeCl_3$. The graphite-$FeCl_3$ data are taken from a previous study by Smith and Eklund[30] and is incorporated for comparison to the graphite-$SbCl_5$ data, and the point at $(1/n)=0$ (HOPG) is due to Taft and Phillip.[25] For a given stage index the plasma frequency data for graphite-$SbCl_5$ lies higher than those for graphite-$FeCl_3$, consistent with a higher charge transfer per C atom in the graphite-$SbCl_5$ compounds. The high-stage $(n \geq 4)$ data can be understood on the basis of a simple model calculation which explains the nearly linear rise of ω_p^2 with increasing $1/n$ ap-

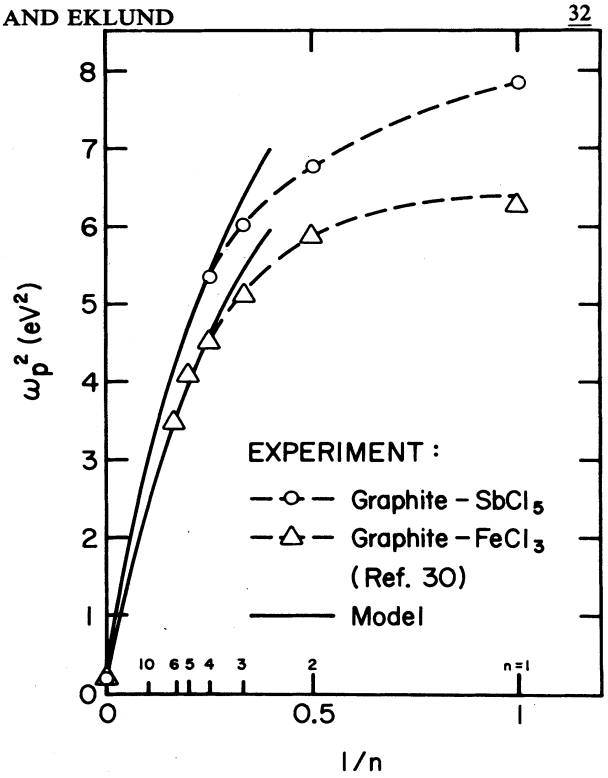

FIG. 7. ω_p^2 vs inverse stage $(1/n)$ for graphite-$SbCl_5$ (this work) and graphite-$FeCl_3$ (Ref. 30). The solid lines indicate the model calculation using Eq. (8). The dashed lines are a guide to the eye.

parent in the figure. In this model we consider separate contributions to the plasma frequency from holes which reside primarily in the bounding (b) C layers and from holes which reside primarily in interior (i) C layers. That is, we write

$$\omega_p^2 = 4\pi e^2 (N_i/m_i + N_b/m_b) , \tag{6}$$

where N_j and m_j $(j=i,b)$ refer, respectively, to the carrier concentration and optical mass of holes in the (i,b) C layers. Writing the carrier concentrations N_j in terms of 2D charge densities ξ_j, we have

$$N_i = (n-2)\xi_i / I_c , \tag{7a}$$

$$N_b = 2\xi_b / I_c , \tag{7b}$$

where I_c is the distance between intercalate layers. Using Eqs. (6) and (7) and approximating the repeat distance by the relation $I_c = D + nd_c$, where D and d_c are the intercalate and carbon layer thickness, respectively, Eq. (6) can be recast as

$$\omega_p^2 = \left[\frac{D}{d_c} + n \right]^{-1} [(n-2)\Omega_i^2 + 2\Omega_b^2] , \tag{8a}$$

where

$$\Omega_i^2 = \frac{4\pi e^2 \xi_i}{m_i d_c} \tag{8b}$$

and

$$\Omega_b^2 = \frac{4\pi e^2 \xi_b}{m_b d_c} . \tag{8c}$$

TABLE I. Parameters determined for the free-carrier (Drude), valence-to-valence interband transition, and valence-to-conduction interband transition contributions to the electronic structure of stage-1–4 graphite-$SbCl_5$. The asterisk (*) denotes contributions due to a slight admixture of stage 2 in the stage-1 sample. The dagger (†) denotes contributions due to a slight admixture of stage 4 in the stage-3 sample.

	Stage 1	2	3	4
Drude				
ω_p (eV)	2.8±0.05	2.6±0.05	2.45±0.05	2.28±0.05
$\omega_p\tau$	75±1	70±1	43±1	68±1
ϵ_∞	6.0±0.5	5.9±0.05	9.0±0.05	10.0±0.05
$V\rightarrow V$				
ω (eV)	$\omega_{21}^*=0.36\pm0.002$	$\omega_{21}=0.375\pm0.002$	$\omega_{32}^\dagger=0.395\pm0.002$	$\omega_{32}=0.40\pm0.002$
Γ (eV)	$\Gamma_{21}^*=0.14\pm0.005$	$\Gamma_{21}=0.12\pm0.005$	$\Gamma_{32}^\dagger=0.06\pm0.005$	$\Gamma_{32}=0.07\pm0.005$
f (eV^2)	$f_{21}^*=0.15\pm0.005$	$f_{21}=0.82\pm0.005$	$f_{32}^\dagger=0.185\pm0.002$	$f_{32}=0.504\pm0.002$
ω (eV)			$\omega_{31}=0.56\pm0.002$	$\omega_{42}=0.52\pm0.002$
Γ (eV)			$\Gamma_{31}=0.14\pm0.005$	$\Gamma_{42}=0.25\pm0.005$
f (eV^2)			$f_{31}=0.875\pm0.002$	$f_{42}=0.75\pm0.005$
ω (eV)			$\omega_{41}^\dagger=0.70\pm0.002$	$\omega_{41}=0.74\pm0.002$
Γ (eV)			$\Gamma_{41}^\dagger=0.25\pm0.005$	$\Gamma_{41}=0.30\pm0.005$
f (eV^2)			$f_{41}^\dagger=0.84\pm0.005$	$f_{41}=1.60\pm0.005$
m_{opt}/m_0	0.24±0.02	0.14±0.02		
$E_F(\omega_p)$ (eV)	1.28±0.05	0.79±0.03		
$E_F(E_T)$ (eV)	0.98±0.01	0.89±0.01	0.71±0.01	0.72±0.01

The solid lines in Fig. 7 are calculated according to Eqs. (8) using the following stage-independent parameters: $\Omega_i=0.44$ eV (graphite[25]), Ω_b is calculated according to Eq. (8a) for $n=4$ to match the data, $D(FeCl_3)=6.09$ Å, and $D(SbCl_5)=6.02$ Å. As can be seen in the figure, the data are well described by this simple calculation.

We next interpret the stage-1 and -2 graphite-$SbCl_5$ plasma frequency data in the framework of the 2D tight-binding band model of Blinowksi and co-workers.[11,12] This model considers nearest-neighbor, in-plane (γ_0) and out-of-plane (γ_1) interactions between C atoms in the carbon layer(s) contained between successive intercalate layers. One virtue of the small number of interactions entertained in their calculations is that analytical expressions can be obtained, relating, for example, charge transfer per carbon atom (f/l), the plasma frequency, and the position of the Fermi level. For the stage-1 compound,[11]

$$\omega_p^2=\frac{4e^2}{\hbar^2 I_c}E_F \quad \text{(stage 1)} \tag{9}$$

and

$$(f/l)=\frac{1}{\pi\sqrt{3}}(E_F/\gamma_0)^2 \quad \text{(stage 1)}\,. \tag{10}$$

Using Eq. (9) we obtain a value of $E_F=1.28\pm0.05$ eV using $I_c=9.42$ Å (Refs. 16 and 17) and the experimental value $\omega_p=2.8\pm0.05$ eV. We note that this value for E_F is independent of the value of γ_0 and is a simple consequence of linear dispersion near the zone corner. de Haas–van Alphen oscillations in stage-1 graphite-$SbCl_5$ observed by Zaleski, Ummat, and Datars[14] are found by them to be in good agreement with the single carbon sheet, linear combination of atomic orbitals (LCAO) calculation of Holzwarth[26] with zone corner π-band dispersion consistent with a value of $\gamma_0=2.9$ eV. Zaleski *et al.* report a value for $E_F=1.127$ eV,[14] which is in good agreement with the present optical results. To determine the charge transfer (f/l) from the plasma frequency, a value for γ_0 must be chosen, however. Recent Shubnikov–de Haas results of Markiewicz and co-workers[31] in a variety of stage-2 acceptor GIC's have been interpreted successfully using a value of $\gamma_0=3.18$ eV, similar to that reported for pristine graphite.[32] We adopt a stage-independent value for γ_0 of 3.0±0.1 eV for the stage-1 and -2 compounds which is roughly midway between that used by Holzwarth[26] and Markiewicz.[31] Stage-dependent values of γ_0 have been reported recently from optical reflectivity studies of graphite-H_2SO_4 by Saint Jean *et al.*[33] They report values for γ_0 of 2.6 and 2.8 eV for stages 1 and 2,[33] respectively. These values lie outside the range of values 3.0±0.1 eV used to interpret the present data. Further optical measurements in the graphite-H_2SO_4 system are underway to resolve the discrepancy.[34]

Using $\gamma_0=3.0\pm0.1$ eV, and the value $E_f=1.28\pm0.05$ eV determined from the plasma frequency [Eq. (10)], we

find a value for $(f/l)=0.033\pm0.005$ holes per C atom. A range of stoichiometry $\sim C_{12-14}SbCl_5$ (Refs. 16 and 17) translates this value into a value $f=0.43\pm0.1$ holes per intercalated unit of $SbCl_5$; a value of $f=\frac{2}{3}$ is anticipated if complete disproportionation of $SbCl_5$ occurs (i.e., 3 $SbCl_5 \rightarrow 2\ SbCl_6^- + SbCl_3$).[15] Thus we find that this process is $\sim 71\%$ complete in the stage-1 compound. The balance of the mass uptake in the intercalate layer is probably in the form of neutral $SbCl_5$.[7] The large uncertainty in f ($\Delta f=\pm0.1$) is due to the superposition of uncertainties in ω_p, γ_0, and the stoichiometry. Magneto-oscillation experiments yield f directly from the orbit area, however.[14] Based on de Haas–van Alphen orbits, Zaleski *et al.* report a value $f=0.37$ for stage-1 graphite-$SbCl_5$, in good agreement with our results.

For the stage-2 compound the expressions relating charge transfer, plasma frequency, and the Fermi level are,[11]

$$\omega_p^2=\frac{8e^2}{\hbar^2 I_c}E_F\left[\frac{E_F^2-\gamma_1^2/2}{E_F^2-\gamma_1^2/4}\right] \quad \text{(stage 2)} \tag{11}$$

and

$$(f/l)=\frac{2}{\pi\sqrt{3}}(E_F/\gamma_0)^2 \quad \text{(stage 2)}\,, \tag{12}$$

where γ_1 is the out-of-plane transfer integral between AB stacked C layers. As discussed previously, an experimental value of $\gamma_1=0.375$ eV is obtained directly from the position of the low-energy $V\rightarrow V$ structure in $\epsilon_2^{\text{bound}}$. Using our value of $\omega_p=2.6\pm0.05$ eV, $I_c=12.72$ Å,[16,17] and $\gamma_1=0.375$ eV in Eq. (12), we find the position of the stage-2 Fermi level at $E_F=0.79\pm0.03$ eV, independent of γ_0. Values of $\gamma_0=3.0\pm0.1$ eV and $E_F=0.79\pm0.03$ eV in Eq. (13) result in a stage-2 value for the number of holes per C atom of $(f/l)=0.026\pm0.003$, which, in conjunction with a stage-2 stoichiometry range of $\sim C_{24-28}SbCl_5$,[16,17] yields a charge transfer per intercalated unit of $SbCl_5$ of $f=0.66\pm0.15$, indicating that disproportionation in the stage-2 compound is 99.4% complete. The large uncertainty in f is due to the uncertainties in γ_0, ω_p, and the stoichiometry. The data indicate that disproportionation is nearly complete in stage 2. We note that if we use a value of 3.18 eV for γ_0, we arrive at a value for $f=0.59$, which is in good agreement with the range of values $0.51<f<0.57$ obtained by Markiewicz[31] for several stage-2 graphite-$SbCl_5$ samples from Shubnikov–de Haas data also using the value $\gamma_0=3.18$ eV. Mössbauer measurements[7] on stage-2 graphite-$SbCl_5$ samples report a $[Sb^{5+}]/[Sb^{3+}]$ ratio of 1.92, which if the Sb^{5+} is primarily in the form of $SbCl_6^-$, as suggested by the narrow Sb^{5+} resonance linewidth,[7] is in excellent agreement with nearly complete disproportionation of stage 2 and our optical results.

For light at near-normal incidence to the c face the optical mass m_{opt} in the Drude form for intraband absorption [Eq. (3)] represents an average of the in-plane dynamical mass over the occupied states,

$$(m_{\text{opt}})^{-1}=\frac{1}{4\pi^3\hbar^2 N}\int_V\left[\frac{\partial^2 E}{\partial k_x^2}\right]d\mathbf{k}\,, \tag{13}$$

where N is the concentration of occupied states associated within the volume V in k space. Using the stage-1 and -2 forms for the electronic dispersion,[11] we find

$$(m_{\text{opt}}/m_0)=\tfrac{4}{9}(\hbar^2 E_F/\gamma_0^2 b^2 m_0) \quad \text{(stage 1)} \tag{14}$$

and

$$(m_{\text{opt}}/m_0)=\tfrac{4}{9}(\hbar^2 E_F/\gamma_0^2 b^2 m_0)\left[\frac{E_F^2-\gamma_1^2/4}{E_F^2-\gamma_1^2/2}\right] \quad \text{(stage 2)}\,, \tag{15}$$

where m_0 is the free-electron mass and b is the in-plane separation between C atoms. Use of the range of values $\gamma_0=3.0\pm0.1$ eV and Fermi-level values obtained from the respective optical plasma frequencies in Eqs. (14) and (15) yields $(m_{\text{opt}}/m_0)=0.24\pm0.02$ (stage 1) and $(m_{\text{opt}}/m_0)=0.14\pm0.02$ (stage 2).

D. Interband absorption

The interband or bound-charge contribution to the dielectric function (or the optical conductivity) is separated from the intraband contribution, as discussed in Sec. III B. The interband contribution for the stage-1–4 GIC's and graphite (HOPG) are plotted as $4\pi\sigma_1^{\text{bound}}=\omega\epsilon_2^{\text{bound}}$ in the bottom panels of Figs. 3(a)–3(e) where σ_1 represents the real part of the optical conductivity. The structure appearing in the data below $\hbar\omega\sim1$ eV in σ_1 is due to transitions between valence bands (Sec. III B). The thresholds for absorption between valence and conduction bands for the stage-1–4 GIC's are observed in σ_1 in the range ~1–1.5 eV, with the thresholds shifting to lower energy with increasing stage index, consistent with a rising Fermi level. For the stage-1–4 compounds the broad peak in σ_1 near ~4.5 eV, which is the GIC analog of the ~5-eV peak in graphite, is identified with the high joint optical density of states near the M point in the Brillouin zone. Very little stage dependence in the position of the M-point peak is observed. The strength of this feature is expected to grow with increasing stage index as indicated in the figures. Energy-band and subsequent dielectric-function calculations in graphite by Johnson and Dresselhaus[32] indicate that second-nearest in-plane C-C interactions are needed to explain quantitatively both the transport data (which is sensitive to the π-band dispersion near the zone corner) and the position of the ~5-eV M-point peak in σ_1 (which is sensitive to the band dispersion along the zone face). A similar band-structure study is needed in the acceptor-type GIC's. At energies a few eV above the M-point absorption we observe a broad feature near 8 eV in the stage-1–4 GIC's which we identify with absorption involving intercalate-derived states. This identification is consistent with the apparent increase in strength of this feature with decreasing stage index or increasing intercalate concentration.

The threshold for $V\rightarrow C$ absorption can be used to estimate the position of the Fermi level on the grounds that the strongest interband matrix elements couple energy bands with approximate mirror symmetry.[11,12] For linear valence- and conduction-band dispersion with mirror

symmetry, the threshold for $V \rightarrow C$ absorption in ϵ_2 takes the form[29]

$$\epsilon_2^{V\rightarrow C}(\omega)=\frac{\pi e^2}{\hbar\omega I_c}\left[\exp\left[\frac{2E_F-\hbar\omega}{2kT}\right]+1\right]^{-1}, \quad (16)$$

where T is the sample temperature. Since mirror symmetry is anticipated for stages 1 and 2, and near mirror symmetry for stages 3 and 4, we use Eq. (16) to obtain values for the position of the Fermi level E_F. In Fig. 8 we display the results of fitting Eq. (16) to the stage-1—4 $V \rightarrow C$ absorption threshold data. The arrows in the figure indicate the position of E_F consistent with the calculated threshold for $\epsilon_2^{V\rightarrow C}$ [Eq. (16)]; the temperatures $T_{\text{eff}} > T$ needed to fit the threshold are also indicated, where $T = 300$ K is the sample temperature. Blinowski *et al.*[11] have attributed the large values of T_{eff} to a lifetime-broadening mechanism. However, weak c-axis dispersion has also been proposed[29] as an alternate explanation for this broadening, as well as the widths of the $V \rightarrow V$ structure. For the stage-1 and -2 compounds we may compare the values of E_F determined from the plasma frequency ω_p and that obtained from the position of the $V \rightarrow C$ threshold E_t. We designate the values of E_F determined from the quantities ω_p and E_t as $E_F(\omega_p)$ and $E_F(E_t)$, respectively, and list the values accordingly in Table I. As indicated in the table for stage 1, we find $E_F(\omega_p)=1.28\pm0.05$ eV and $E_F(E_t)=0.98\pm0.02$ eV; for stage 2 we find $E_F(\omega_p)=0.79\pm0.03$ eV and $E_F(E_t)=0.89\pm0.02$ eV.

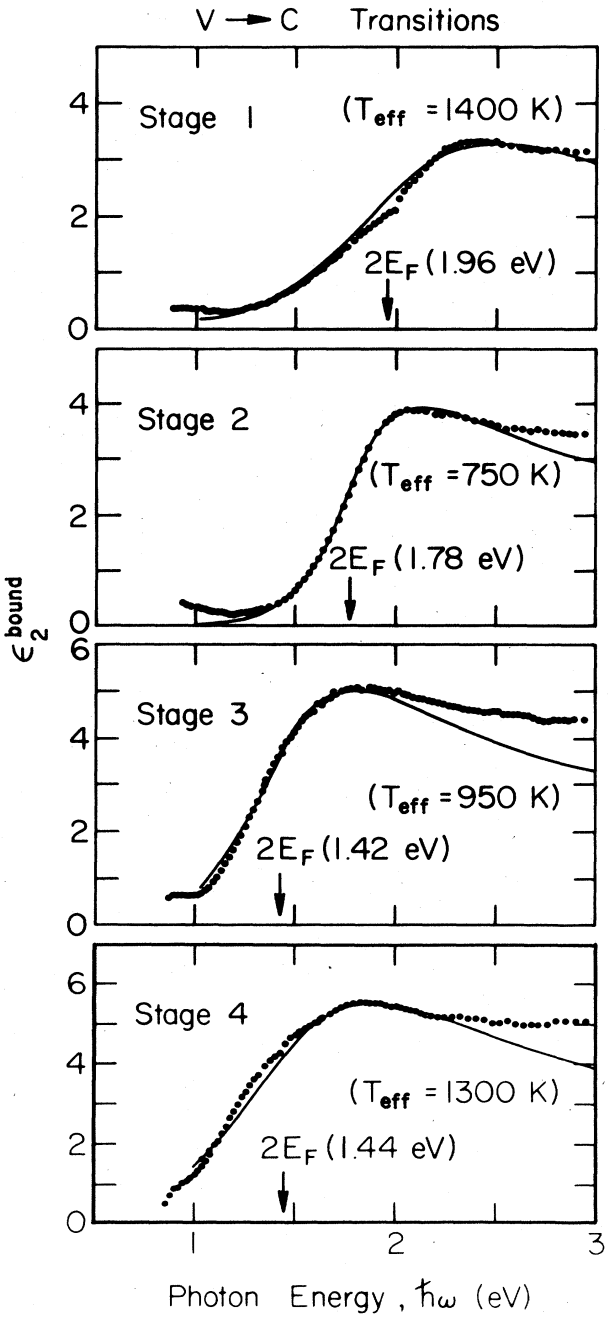

FIG. 8. ϵ_2 in the valence-to-conduction interband transition threshold region. The dots represent $\epsilon_2^{\text{bound}}$ and the solid line is calculated using Eq. (16).

As we have discussed in Sec. III B, the valence-band—to—valence-band ($V \rightarrow V$) absorption is easily separated from the intraband contribution because the $V \rightarrow V$ structure is sharp. The $V \rightarrow V$ contributions to $\epsilon_2^{\text{bound}}$ for the stage-2—4 graphite-$SbCl_5$ compounds are shown in Figs. 5(a)—5(c). The stage-2 data shown in Fig. 5(a) are seen to exhibit an asymmetric peak in ϵ_2 with a sharp maximum near 0.375 eV. Other optical studies have reported $V \rightarrow V$ structure near this value in stage-2 acceptor compounds.[20,30,33] The solid line in the figure represents the Lorentzian line shape [Eq. (5)] used to fit the data (dots). The stage-3 and -4 $V \rightarrow V$ interband contributions are shown in Figs. 5(b) and 5(c), where the data are represented by dots, the solid line represents the sum of the individual Lorentzian functions, and the dashed lines represent the individual Lorentzians. In the stage-3 compound one strong $V \rightarrow V$ feature is predicted by band-structure and matrix-element calculations,[12,13] and we identify the 0.56-eV peak in Fig. 5(b) with this feature. By comparison of Fig. 5(b) (stage 3) and Fig. 5(c) (stage 4), we are compelled to identify the 0.395- and 0.070-eV peaks in the stage-3 data with the presence of coexisting stage-4 material. The stage-3 value of 0.56 eV is in good agreement with the self-consistent calculations of Ohno *et al.*[13] for a charge transfer $f=0.36$ holes per unit $SbCl_5$, and in reasonable agreement with calculations by Blinowski and Rigaux[12] for the case $\delta=\gamma_1/3$, where the parameter δ adjusts the distribution of charge between interior and bounding carbon layers. Other stage-3 graphite-$SbCl_5$ samples have shown substantially reduced 0.395- and 0.70-eV peaks relative to the 0.57-eV peak. Optical reflectivity studies of graphite-H_2SO_4 also report a strong feature near 0.57 eV in the stage-3 compound.[33] The stage-4 data in Fig. 5(c) are seen to contain three peaks, at 0.40, 0.52, and 0.74 eV. These energies are in good agreement with the 2D calculations of Ohno *et al.*[13] and of Blinowski and Rigaux[12] for the case $\delta=\gamma_1/2$. The values of the Lorentzian parameters used to generate the solid curves in Figs. 5(a)—5(c) are listed in Table I. Numbering the valence bands as V_j, consistent with the schematic band structure shown in Fig. 4, the appropriate

energy-band differences $V_{jk}=V_j-V_k$ for the stage-2—4 graphite-$SbCl_5$ compounds may therefore be obtained and are indicated in Table I.

IV. CONCLUSIONS

In this paper we have shown that absolute reflectance spectra of acceptor-type GIC's may be quantitatively analyzed to determine a variety of parameters relevant to the charge transfer and electronic band structure of these materials, such as valence-band energy differences near the Brillouin-zone corner, the position of the Fermi level and the π-band gap near the zone face (M point), and the optical mass. The position of low-energy ($\hbar\omega < 1$ eV) valence-band—to—valence-band absorption in the stage-2—4 spectra are found to be in reasonably good agreement with 2D energy-band model calculations.

ACKNOWLEDGMENTS

We would like to thank A. W. Moore of Union Carbide for the HOPG used in the course of this work. The research was supported, in part, by grants from the U. S. Department of Energy No. DE-FG05-84ER45151) and American Cyanamid. Helpful discussions with Professor K. Subbaswamy are gratefully acknowledged. We would like to thank Pierre Charron for his assistance in the construction of the vacuum-ultraviolet spectrometer.

---

*Present address: SPEX Industries, Edison, NJ 08820.

[1]M. S. Dresselhaus and G. Dresselhaus, Adv. Phys. **30**, 139 (1981).

[2]S. A. Solin, Adv. Chem. Phys. **49**, 455 (1982).

[3]V. R. K. Murthy, D. S. Smith, and P. C. Eklund, Mater. Sci. Eng. **45**, 77 (1980).

[4]See recent results in Summary Report of Project No. 5612207 of the Ministry of Education, Science and Culture, Japan, 1984 (unpublished).

[5]N. Bartlett, R. N. Biagioni, B. W. McQuillan, A. S. Robertson, and A. C. Thompson, J. Chem. Soc., Chem. Commun. 200 (1978).

[6]L. B. Ebert, D. R. Mills, and J. C. Scanlon, Mater. Res. Bull. **18**, 1505 (1983).

[7]P. Boolchand, W. J. Bresser, D. McDaniel, K. Sisson, V. Yeh, and P. C. Eklund, Solid State Commun. **40**, 1049 (1981).

[8]D. H. McDaniel, P. Boolchand, W. J. Bresser, and P. C. Eklund, in *Intercalated Graphite,* edited by M. S. Dresselhaus, G. Dresselhaus, J. E. Fischer, and M. J. Moran, Materials Research Society Symposia Proceedings, Vol. 20 (Elsevier—North Holland, New York, 1983), p. 377.

[9]M. J. Moran, G. R. Miller, R. A. DeMarco, and H. A. Resing, J. Phys. Chem. **88**, 1580 (1984).

[10]D. M. Huang, X. W. Qian, and S. A. Solin, Phys. Rev. Lett. **53**, 1473 (1984).

[11]J. Blinowski, Nguyen Hy Hau, C. Rigaux, J. P. Vieren, R. LeToullec, G. Furdin, A. Herold, and J. Melin, J. Phys. (Paris) **41**, 47 (1980).

[12]J. Blinowski and C. Rigaux, J. Phys. (Paris) **41**, 667 (1980).

[13]T. Ohno, N. Shima, and H. Kamimura, Solid State Commun. **44**, 761 (1982).

[14]H. Zaleski, P. K. Ummat and W. R. Datars, J. Phys. C **17**, 3167 (1984).

[15]M. S. Dresselhaus and G. Dresselhaus, in *Light Scattering in Solids III,* edited by M. Cardona and G. Güntherodt (Springer, Berlin, 1982), Chap. 2.

[16]J. Melin and A. Herold, C. R. Acad. Sci. **269**, 877 (1969).

[17]M. H. Boca, M. L. Saylors, D. S. Smith, and P. C. Eklund, Synth. Met. **6**, 39 (1983).

[18]See for example C. H. Olk, F. J. Holler, and P. C. Eklund, in *Intercalated Graphite,* Ref. 8, p. 259.

[19]J. Giergiel, Ph.D. thesis, University of Kentucky, 1982 (unpublished).

[20]P. C. Eklund, D. S. Smith, and V. R. K. Murthy, Synth. Met. **3**, 111 (1981).

[21]F. Wooten, *Optical Properties of Solids* (Academic, New York, 1972), p. 248.

[22]F. Wooten, *Optical Properties of Solids,* Ref. 21, p. 90.

[23]A. Zunger, Phys. Rev. B **17**, 626 (1978).

[24]F. Wooten, *Optical Properties of Solids,* Ref. 21, p. 249.

[25]E. A. Taft and H. R. Phillip, Phys. Rev. **138**, A197 (1965).

[26]N. A. Holzwarth, Phys. Rev. B **21**, 3665 (1980).

[27]G. Dresselhaus and S. Y. Leung, Solid State Commun. **35**, 819 (1980).

[28]R. S. Markiewicz, Solid State Commun. **44**, 791 (1982).

[29]D. M. Hoffman, P. C. Eklund, R. E. Heinz, P. Hawrylak, and K. R. Subbaswamy, Phys. Rev. B **31**, 3973 (1985).

[30]D. S. Smith and P. C. Eklund, in *Intercalated Graphite,* Ref. 8, p. 99.

[31]R. S. Markiewicz, C. Lopatin, and C. Zahopoulos, in *Intercalated Graphite,* Ref. 8, p. 135.

[32]L. G. Johnson and G. Dresselhaus, Phys. Rev. B **7**, 2275 (1973).

[33]M. Saint Jean, M. Menant, Nguyen Hy Hau, C. Rigaux, and A. Metrot, Synth. Met. **8**, 189 (1983).

[34]J. M. Zhang, D. M. Hoffman, and P. C.Eklund (unpublished).